

11102-OR
121470
119

**ROTATIONAL AND VIBRATIONAL NONEQUILIBRIUM EFFECTS
IN RAREFIED, HYPERSONIC FLOW**

**ORIGINAL PAGE IS
OF POOR QUALITY**

Iain D. Boyd *
Eloret Institute
NASA Ames Research Center
Moffett Field, CA 94035

Abstract

Results are reported for an investigation into the methods by which energy transfer is calculated in the Direct Simulation Monte Carlo method. Description is made of a recently developed energy exchange model that deals with the translational and rotational modes. A new model for simulating the transfer of energy between the translational and vibrational modes is also explained. This model allows the vibrational relaxation time to follow the temperature dependence predicted by the Landau-Teller theory at moderate temperatures. For temperatures in excess of about 8000K the vibrational model is extended to include an empirical result for the relaxation time. The effect of introducing these temperature dependent collision numbers into the DSMC technique is assessed by making calculations representative of the stagnation streamline of a hypersonic space vehicle. Both thermal and chemical nonequilibrium effects are included while the flow conditions have been chosen such that ionization and radiation may be neglected. The introduction of these new models is found to significantly affect the degree of thermal nonequilibrium observed in the flowfield. Larger, and more widely ranging, differences in the results obtained with the different energy exchange probabilities are found when a significant amount of internal energy is included in the calculation of chemical nonequilibrium.

Nomenclature

- AOTV = Aero-assisted Orbital Transfer Vehicle
- \bar{c} = average molecular velocity
- C_H = heat-transfer coefficient
- $f(g)$ = relative velocity distribution function
- g = relative velocity of collision
- g^* = characteristic velocity
- m_r = reduced mass of collision
- n = number density
- T = translational temperature
- T^* = characteristic temperature for Z_R
- T_{ref} = reference temperature for VHS model
- VHS = Variable Hard Sphere

- X_i = mass fraction for species i
- Z_R = rotational collision number
- $(Z_R)_\infty$ = infinite temperature collision number
- Z_t = translational collision number
- ϕ_R = probability of rotational energy exchange
- ϕ_v = probability of vibrational energy exchange
- ν = molecular collision rate
- ω = parameter in VHS model
- σ_{ref} = reference collision cross section for VHS model
- σ_v = effective excitation cross section
- τ_{LT} = Landau-Teller vibrational relaxation time
- τ_P = Park's empirical correction for relaxation time
- τ_v = total vibrational relaxation time

Introduction

The Direct Simulation Monte Carlo method (DSMC) developed by Bird¹ is an important numerical technique for the calculation of low density flowfields. The method simulates the flow at the molecular level by calculating collisions on a probabilistic basis. One of the most important aspects of DSMC calculations is the ability to model thermal nonequilibrium in which the temperatures associated with the various energy modes of the gas (translational, rotational, vibrational, electronic) are unequal. In order to reduce computational overheads, such phenomena are usually modelled in a simplistic manner in which the probability of energy exchange between these various modes is a constant for each type of transfer mechanism. If a particular collision is accepted for internal energy transfer, then post collision values are sampled from the local equilibrium distribution function in accordance with the Larsen-Borgnakke phenomenological model².

By employing this energy exchange scheme, significant degrees of thermal nonequilibrium have been calculated for expansions in plumes^{3,4} and for compressions in shock waves^{5,6}. Recently, one of the most interesting applications of the DSMC technique has been to the flowfield surrounding a hypersonic space vehicle such as the Space Shuttle or an Aero-Assisted Orbital Transfer Vehicle (AOTV) as de-

* Research Scientist, Member AIAA

scribed in Refs. 5 and 6. The degree of thermal nonequilibrium in such energetic flows can have a significant impact on the shock standoff location, on the amount of chemical activity, and on the convective and radiative heat load to the vehicle. It is therefore of great importance that the models employed in the calculation of energy transfer be physically realistic. For AOTV calculations the probabilities assumed for rotational and vibrational energy exchange are usually taken to be 0.2 and 0.02 respectively. The value for the transfer of rotational energy has been derived from experimental studies for temperatures of about 1000K. In the case of vibrational energy exchange, the probability of 0.02 is an estimate of the maximum possible. In reality, the probability of energy transfer would be expected to be much smaller except at very high temperatures. It is the purpose of the present work to describe the procedures for implementing energy transfer probabilities which are dependent upon the local translational temperature. Rather than calculating the translational temperature at each cell in the simulation and then employing continuum expressions to evaluate the relaxation time⁷, each probability of energy exchange is obtained by integrating over all simulated collisions. This procedure should ensure that any nonequilibrium attributes associated with the translational modes are incorporated into the calculation. The effect of introducing such expressions into the DSMC technique is assessed by making one-dimensional calculations along the stagnation streamline of a hypersonic vehicle. First, the methods for calculating the probability of internal energy transfer are described.

Probability of Rotational Energy Transfer

The following approximate expression for the rotational collision number was obtained by Parker⁸

$$Z_R = \frac{(Z_R)_\infty}{1 + \frac{\pi^{\frac{1}{2}}}{2} \left(\frac{T^*}{T}\right)^{\frac{1}{2}} + \left(\frac{\pi^2}{4} + \pi\right) \frac{T^*}{T}} \quad (1)$$

where T^* is the characteristic temperature of the intermolecular potential, and $(Z_R)_\infty$ is the limiting value. While Parker's expression is derived from an analysis involving a large number of assumptions, the temperature dependent nature of Eq.(1) is in agreement with the more rigorous treatment of Lordi and Mates⁹ who performed classical trajectory calculations. In the current work the value of $(Z_R)_\infty$ is chosen so as to obtain the best correspondence between Parker's results and those of Lordi and Mates. To incorporate Parker's continuum formula into the DSMC technique an expression for the probability of energy transfer must be developed as a function of the relative collision velocity.

This expression must reduce to Eq.(1) when integrated over all possible collisions. Such a formulation has been derived in Ref. 10 and is given as

$$\phi_R \frac{(Z_R)_\infty}{Z_t} = 1 + \frac{\Gamma(2-\omega)}{\Gamma(\frac{3}{2}-\omega)} \left(\frac{2kT^*}{m_r g^2}\right)^{\frac{1}{2}} \frac{\pi^{\frac{1}{2}}}{2} + \frac{\Gamma(2-\omega)}{\Gamma(1-\omega)} \left(\frac{2kT^*}{m_r g^2}\right) \left(\frac{\pi^2}{4} + \pi\right) \quad (2)$$

where ϕ_R is the probability of energy transfer between the translational and rotational modes, Z_t is the translational collision number, m_r is the reduced mass of collision, and g is the relative collision velocity. In the derivation of Eq.(2) the Variable Hard Sphere collision model of Bird¹¹ has been employed in which the molecular collision rate is given by

$$\nu = \frac{2n\sigma_{ref}}{\sqrt{\pi}} \Gamma(2-\omega) \left(\frac{2kT}{m_r}\right)^{\frac{1}{2}} [(2-\omega)T_{ref}/T]^\omega \quad (3)$$

where n is the number density, σ_{ref} defines a collision cross section at a temperature T_{ref} , and ω defines the interaction potential. In a separate set of calculations¹⁰, Eq.(2) was employed in the calculation of a standing shock wave and the results obtained were found to offer better correspondence to the experimental data than those with $\phi_R=0.2$. It has been found by Belikov et al¹² that Parker's formulation appears to give the correct behavior up to about 4000K. In addition, it has been shown by Lumpkin et al¹³ that Eq.(1) gives good agreement with experimental shock wave thickness for a range of Mach number. Indeed, in Ref. 13 it is observed that Parker's simple formulation provides better correspondence than the results obtained with calculations which employed a more sophisticated model based on rotational transition rates. As shown in Fig. 1, even at 1000K the probability of rotational energy transfer for nitrogen is certainly different to 0.2 and the variation in ϕ_R will therefore have some impact on the calculated results. When Eq.(2) is evaluated at each collision, it is found that equipartition of the thermal modes is not achieved due to the fact that the collision probability is biased towards those collisions having smaller translational energies. The mean collision probability for each cell in the computational domain is therefore employed, and is obtained by averaging Eq.(2) over all collisions.

Probability of Vibrational Energy Transfer

In a pure gas of diatomic molecules, the mean probability of vibrational-translational energy exchange may be expressed as

$$\overline{\phi_v} = \frac{1}{\tau_v \nu} = \int_{-\infty}^{\infty} \phi_v(g) f(g) dg \quad (4)$$

where ϕ_v is the probability of energy exchange for the collision with relative velocity g , $f(g)$ is the relative velocity distribution function, and τ_v is the vibrational relaxation time. In the following, we wish to choose a form for ϕ_v such that the vibrational relaxation time is given by the expression obtained by Millikan and White¹⁴ who correlated a number of experimental results. The probability of energy exchange is assumed to be of the form

$$\phi_v = \frac{1}{Z_o} g^\alpha \exp\left(\frac{-g^*}{g}\right) \quad (5)$$

where α and Z_o are constants, and g^* is a characteristic velocity. The form of Eq.(5) is identical to that originally assumed by Landau-Teller with α set equal to zero. The integral obtained by substituting Eq.(5) into Eq.(4) can only be evaluated approximately using the method of steepest descent¹⁵. The result obtained with this method reveals that the temperature dependent nature of the vibrational collision number is obtained when

$$\alpha = 3 - 2\omega \quad (6)$$

A detailed description of the preceding analysis together with the expressions for the constant Z_o in Eq.(5) and the characteristic velocity g^* are included in Ref. 15. For a hard sphere interaction ($\omega=0$), the instantaneous probability of vibrational-translational energy exchange for nitrogen is

$$\phi_v = 1.20 \times 10^{-11} g^3 \exp\left(-\frac{43300}{g}\right) \quad (7)$$

Results obtained with the DSMC technique employing Eq.(7) are plotted in Fig. 2 together with the continuum result. Due to the approximation used in evaluating Eq.(4), the results are not identical, with the DSMC results always lying less than a factor of 2 above the exact solution.

The vibrational relaxation time of Millikan and White is generally recognized to be valid up to temperatures of about 8000K. In the consideration of hypersonic flow surrounding space vehicles, the translational temperature may be as high as 40,000K. To better simulate the vibrational-translational exchange process at such elevated temperatures Park¹⁶ introduced the following empirical correction

$$\tau_v = \tau_{LT} + \tau_p \quad (8)$$

where τ_{LT} is the Landau-Teller relaxation time,

$$\tau_p = \frac{1}{n\sigma_v\bar{c}} \quad (9)$$

σ_v is the effective excitation cross-section and \bar{c} is the average molecular velocity. This correction to the vibrational collision number may be evaluated in a similar manner to that employed for rotational-translational energy exchange. If the excitation cross-section is taken to be constant, then the following expression is obtained

$$\phi_p = \frac{\sigma_v}{\sqrt{2}\sigma_{ref}} \frac{1}{\Gamma(2-\omega)} [T/(2-\omega)T_{ref}]^\omega \quad (10)$$

An expression which reduces to Eq.(10) when integrated over all collisions is

$$\phi_p = \frac{\sigma_v}{\sqrt{2}\sigma_{ref}} \left[\frac{m_r g^2}{2(2-\omega)kT_{ref}} \right]^\omega \quad (11)$$

It should be noted that it is possible to include a temperature dependent form for σ_v if desired. From Eq.(11) it is seen that for hard spheres, the result is independent of the collision velocity. Park's modification to the vibrational relaxation time is implemented in the DSMC method by averaging Eq.(11) over all collisions. To ensure that the integration is being performed correctly, the results for $\omega=0.25$ and nitrogen molecules are shown in Fig. 3 for the modified vibrational relaxation time of Eq.(8). It is seen that the DSMC and continuum results are in excellent agreement.

Calculations

Having derived expressions which allow both the rotational and vibrational collision numbers to vary with temperature, the effect of introducing these developments into energetic DSMC calculations is now assessed. The problem chosen for consideration is the flow along the stagnation streamline in front of a hypersonic space vehicle. The solution procedure follows that of Bird¹⁷ who has shown that the stagnation streamline flow may be reduced to one dimension. One end of the computational domain is open through which enter molecules representative of the upstream conditions. At the opposite end is the surface of the space vehicle, which is assumed to be a diffuse reflector with full energy accommodation. As the molecules are reflected back from the wall a shock wave forms which gradually moves away from the surface. A steady flow is achieved by removing molecules from a downstream portion of the flow with probability proportional to the square of the normal velocity component. This procedure has been shown to conserve energy and momentum when the molecules are removed in the region lying between the shock standoff location and the surface.

The conditions investigated represent the exit of the space vehicle through the atmosphere rather than the reentry. The exit phase is significantly less energetic than reentry and allows us to neglect ionization and radiation effects

in the calculations. An altitude of 90km has been selected and the free stream flow conditions are listed in Table 1. The wall surface is assumed to be constant at 1000K and is non-catalytic. A five species gas mixture is employed (N_2 , O_2 , NO , N , O) with 19 different chemical reactions (see Table 2(a), Ref. 18). Due to the low densities involved, recombination reactions have been omitted from the analysis. Calculations have been completed for three different cases. The first of these follows the previous work by setting $\phi_R=0.2$ and $\phi_V=0.02$. Secondly, the temperature and species dependent expression in Eq.(2) for rotational energy transfer is introduced. Finally, both the rotational and the vibrational energy exchange probabilities are calculated as a function of temperature and molecular species using Eq.(2) and Eqs.(6,11). Details of the parameters used in the energy exchange models are given in Table 2 for rotation, and in Table 3 for vibration. The value for the translational relaxation number Z_t , required in Eq.(2), is that proposed by Fritzsche and Cukrowski¹⁹.

While the primary focus of the present work is the investigation of thermal nonequilibrium effects, the importance of chemical nonequilibrium cannot be ignored. Initially, rotational energy contributions to the energy available for reaction are only included on a restricted basis, and where required by Bird's steric factor for the VHS model. The fractions of rotational energy allowed to participate in the various reactions are those employed by Bird²⁰ in his general purpose code. The effect of this assumption on the flowfield is also analysed by allowing all of the rotational energy available in each collision to be incorporated into the steric factor. For the dissociation reactions it would of course be more realistic to include contributions from the vibrational modes. Unfortunately, the implementation of such a procedure is numerically expensive when Bird's steric factor is employed. It is proposed that the use of the rotational energy will at least give an indication of the importance of including internal energy contributions in the calculation of chemical nonequilibrium.

Results and Discussion

At an altitude of 90km, Ref. 16 shows that the shock standoff distance, which is defined as the point at which the local density is 6 times the free stream value, is located at a distance of 0.11m from the vehicle surface. The present calculations have been performed by forcing the standoff distance to be 0.11m for the case where the exchange probabilities are constant. The other cases are then run under identical conditions such that the steady state is introduced at the same point in the simulation. This allows investiga-

tion of any movement in the standoff distance in the various calculations undertaken. In Fig. 4a, the temperature profiles along the stagnation streamline are plotted for the case in which the probabilities of rotational and vibrational energy exchange are both kept constant. As expected, a significant degree of nonequilibrium exists, with the translational mode reaching a peak temperature of about 25,000K. The results shown offer excellent agreement with the profiles reported in Refs. 5 and 6. The variation along the stagnation streamline of the mass fraction of each of the five species is shown in Fig. 4b for the same case. A significant amount of chemical activity is observed in the flowfield.

Let us now consider the effect of introducing a temperature and species dependent rotational energy exchange probability into the calculations. In Fig. 5 the rotational temperature profiles obtained with the two different modelling methods are shown. It is found that the maximum rotational temperature attained is significantly reduced for the case of the variable exchange probability. This effect may be explained by examination of Fig. 6 in which the rotational probabilities obtained in the calculations are shown for each of the three molecular species. It may be seen from Fig. 4b that molecular nitrogen dominates the flow, so let us concentrate on this data. At the relatively low free-stream temperature, the probability of rotational energy transfer is very close to the nominal value of 0.2 and gradually decreases as the translational temperature increases. It should be noted that the energy exchange probability increases again as the cooling effects of the vehicle surface become important. The values of the exchange probabilities for oxygen are observed to be everywhere greater than those for nitrogen with a maximum of about 0.29 at the free-stream boundary. For nitric oxide, a value for the exchange probability is not obtained until a distance of about 0.2 from the vehicle. This is explained by the fact that, up to this point, NO gas exists in insufficient quantities to produce any collisions in the simulation. As the rotational energy exchange probability is quite large at the upstream boundary for both the nitrogen and oxygen molecules then it might be expected that the rotational temperature in Fig. 4a would lie closer to the translational result at this location. However, Fig. 7 reveals that the various thermal modes are in fact in equilibrium at the upstream location for nitrogen, and this is also found to be the case for the oxygen molecules. Examination of the results obtained for each species revealed that the large translational temperature obtained in Fig. 4a at the upstream boundary is caused by a very small fraction of highly energetic, backscattered atoms and nitric oxide molecules.

In Fig. 8, the vibrational temperature profiles are shown for the two energy exchange probability models. As in the case of rotational relaxation, it is found that the maximum vibrational temperature is significantly reduced. The individual exchange probabilities for each molecular species are plotted in Fig. 9. Careful attention should be given to the labelling of the axes. Only a portion of the domain modelled along the stagnation streamline is included. Beyond distances of about 0.25m from the vehicle, the collision rate is too low to allow any vibrational energy exchange for the variable probability model. It is to be remembered that the DSMC technique employs a discrete number of simulated molecules in the simulation which undergo a discrete number of collisions. For calculated exchange probabilities which are very small, e.g. 10^{-4} , it is therefore difficult to accurately resolve the exchange phenomenon. In direct contrast to the results found for the rotational exchange probabilities, the maximum translational temperature gives rise to the maximum exchange probabilities. For both nitrogen and oxygen these maximum values fall well below 0.02 which is the value previously assumed. It is satisfying to note that the values for nitric oxide lie well above those of the other molecules. This is the trend expected from experiment, and shows that such behavior can now be incorporated into the DSMC calculations through application of the variable exchange probability model.

It is therefore found that the introduction of the variable exchange probabilities leads to a greater degree of thermal nonequilibrium in the flow due to the fact that the calculated probabilities are always much smaller than the values of 0.2 and 0.02 normally assumed for energy exchange with the rotational and vibrational modes respectively. However, at the macroscopic level, only a small effect is observed through the introduction of the temperature dependent models. One example is shown in Fig. 10 where the mass fraction of molecular and atomic nitrogen is compared. It is seen that a greater amount of nitrogen atoms are produced in the case where variable probabilities are employed. In Table 4 various results obtained from these simulations are shown. It is found that both the shock standoff distance and the heat coefficient increase slightly with the introduction of first the variable rotational exchange probability, and then additionally for the corresponding model for vibration.

It is perhaps surprising that the introduction of the new models has had such little effect on the important flow quantities. However, this is almost certainly due to the fact that the internal energy modes are only included in the chemical nonequilibrium phenomenon on a restricted basis. At a time when the significant role of internal energy in chem-

ical nonequilibrium has been incorporated into continuum calculations^{21,22} it is unsatisfactory for the discrete particle solution methods to lag behind in this area. There is a real requirement for improvement in the modelling of chemical reactions in the DSMC technique. In an attempt to assess the effect of the particular chemical model employed, the same flow conditions have been recalculated with the total rotational energy now being available for reaction.

In Fig. 11, the mass fraction of molecular nitrogen is shown for the cases where constant exchange probabilities were employed for both rotational and vibrational energy. It is seen that a reduced amount of dissociation is found for the increased internal energy contribution. This would be expected as Bird's steric factors assume perfect equilibrium for the various thermal modes. Therefore, when the internal temperatures lie below the translational result, which is the case for the flow along most of the stagnation streamline, a smaller rate of reaction will occur.

The thermal nonequilibrium effects discussed above for the restricted rotational energy contribution to chemical reactions were repeated in the new set of calculations. However, larger differences for other flow quantities were discernible. In Fig. 12 are shown the mass fractions for atomic and molecular oxygen for the two cases where constant and variable exchange probabilities were employed. There is a smaller amount of molecular oxygen present in the mixture when the variable models are introduced. Similar behavior is observed for nitrogen, as shown in Fig. 13, but to a lesser extent. The exact explanation for these trends is complicated by the presence of the number of competing reactions which are accounted for in the calculations. The differences between the solutions obtained with the variable exchange probabilities are now large enough to be noticed in such macroscopic quantities as density and velocity which are plotted in Figs. 14 and 15 respectively. It is found that the density is greater for the variable probability calculations in the region lying between the free stream and the shock standoff location. Thereafter, the variable result is slightly below that obtained with the constant probability. In Fig. 15, it is seen that the velocity solutions obtained with the different methods are clearly different with the variable result lagging behind. These findings are of a similar magnitude to the differences noted by Moss et al in Ref. 18 for different sets of chemical reaction rate constants. It is therefore found that further uncertainty in such calculations arises from the techniques employed in the simulation of thermal and chemical nonequilibrium effects.

Various global results obtained with these calculations

are compared in Table 5 with that previously obtained for the constant exchange probabilities. The assumption of a full rotational energy contribution for chemical reactions results in an increased effect through the inclusion of the variable energy exchange probability models. The heat-transfer coefficient, the mass fraction of molecular nitrogen at the surface, and the shock standoff distance are all affected for the different modelling methods.

Concluding Remarks

The calculations reported show that the introduction of temperature and species dependent internal energy exchange probabilities into DSMC calculations can have significant impact on the results obtained. The constant values normally employed for rotational and vibrational energy transfer are generally larger than the values calculated in the simulation. The degree of thermal nonequilibrium is therefore increased due to a reduction in the amount energy transfer performed. Indeed, the vibrational exchange probabilities obtained for nitrogen are an order of magnitude smaller than the constant value previously assumed.

The differences observed in other flow quantities for the different energy exchange models are found to be largest when the internal modes are allowed to contribute a significant amount of energy to that available for each chemical reaction. In the current investigation only the rotational energy contribution has been considered, and is found to be important. In the case where the total rotational energy is included in the collision energy, the variable energy exchange models are found to have a pronounced effect on such important quantities as the shock standoff distance and the heat-transfer coefficient.

It is concluded that consideration should be given to the implementation of the energy transfer probabilities described in this paper. It is probable that the effects observed in the present calculations will be more pronounced for the more energetic flowfields associated with atmospheric reentry of an AOTV or Mars return vehicles. It is a requirement for the future to investigate such conditions and to consider in detail the role of chemical nonequilibrium in such flows. In addition, the role of the variable exchange probabilities in expanding flows, such as that around the aerobrake skirt of an AOTV, should be considered. In such flow, the freezing of the vibrational temperature plays a significant role in the determination of radiation effects.

Acknowledgement

The author gratefully acknowledges the information supplied by Dr.J.N.Moss on the one-dimensional calcula-

tions previously undertaken at NASA Langley for the flow along the stagnation streamline of the Space Shuttle Orbiter.

References

- ¹ Bird, G.A., *Molecular Gas Dynamics*, Clarendon Press, Oxford, 1976.
- ² Borgnakke, C. and Larsen, P.S., "Statistical Collision Model for Monte Carlo Simulation of Polyatomic Gas Mixtures", *Journal of Computational Physics*, Vol. 18, 1975, pp. 405-420.
- ³ Hueser, J.E., Melfi, L.T., Bird, G.A., and Brock, F.J., "Rocket Nozzle Lip Flow by Direct Simulation Monte Carlo Method", *Journal of Spacecraft and Rockets*, Vol. 23, No. 4, 1986, pp. 363-367.
- ⁴ Boyd, I.D. and Stark, J.P.W., "Assessment of Impingement Effects in the Isentropic Core of a Small Satellite Control Thruster Plume", to appear in *Proceedings of the Institution of Mechanical Engineers, Part G: Journal of Aerospace Engineering*.
- ⁵ Moss, J.N. and Bird, G.A., "Direct Simulation of Transitional Flow for Hypersonic Reentry Conditions", in *Thermal Design of Aeroassisted Orbital Transfer Vehicles*, edited by H.F. Nelson, Volume 96 of Progress in Astronautics and Aeronautics, AIAA, New York, 1985, pp. 113-139.
- ⁶ Dogra, V.K., Moss, J.N., and Simmonds, A.L., "Direct Simulation of Stagnation Streamline Flow for Hypersonic Reentry", AIAA Paper 87-0405, Reno, January 1987.
- ⁷ Olynick, D., Moss, J.N. and Hassan, H., "Influence of Afterbodies on AOTV Flows", AIAA Paper 89-0311, January 1989.
- ⁸ Parker, J.G., "Rotational and Vibrational Relaxation in Diatomic Gases", *Physics of Fluids*, Vol. 2, No. 4, 1959, pp. 449-462.
- ⁹ Lordi, J.A. and Mates, R.E., "Rotational Relaxation in Nonpolar Diatomic Gases", *Physics of Fluids*, Vol. 13, No. 2, 1970, pp. 291-308.
- ¹⁰ Boyd, I.D., "Rotational-Translational Energy Transfer in Rarefied Nonequilibrium Flows", submitted for publication.
- ¹¹ Bird, G.A., "Monte Carlo Simulation in an Engineering Context", in *Rarefied Gas Dynamics*, edited by Sam S. Fisher, Volume 74 of Progress in Astronautics and Aeronautics, Part I, AIAA, New York, 1981, pp. 239-255.
- ¹² Belikov, A.E., Sharafutdinov, R.G. and Sukhinin, G.I., "Nitrogen Rotational Relaxation Time Measured in Free Jet", to appear in Proceedings of the 16th International Symposium on Rarefied Gas Dynamics, Progress in Astronautics and Aeronautics, AIAA, Washington, 1989.

- ¹³ Lumpkin, F.E., Chapman, D.R., and Park, C., "A New Rotational Relaxation Model for Use in Hypersonic Computational Fluid Dynamics", AIAA Paper 89-1737, Buffalo, June 1989.
- ¹⁴ Millikan, R.C. and White, D.R., "Systematics of Vibrational Relaxation", *Journal of Chemical Physics*, Vol. 39, No. 12, 1963, pp. 3209-3213.
- ¹⁵ Boyd, I.D., "Calculation of Vibrational Energy Exchange Using Discrete Particle Simulation Methods", submitted for publication.
- ¹⁶ Park, C., "Problems of Rate Chemistry in the Flight Regimes of Aeroassisted Orbital Transfer Vehicles", in *Thermal Design of Aeroassisted Orbital Transfer Vehicles*, edited by H.F. Nelson, Volume 96 of Progress in Astronautics and Aeronautics, AIAA, New York, 1985, pp. 511-537.
- ¹⁷ Bird, G.A., "Direct Simulation of Typical AOTV Entry Flows", AIAA Paper 86-1310, June 1986.
- ¹⁸ Moss, J.N., Bird, G.A. and Dogra, V.K., "Nonequilibrium Thermal Radiation for an Aeroassist Flight Experiment Vehicle", AIAA Paper 88-0081, January 1988.
- ¹⁹ Fritzsche, S. and Cukrowski, A.S., "Relaxation of Translational Energy in Perpendicular Directions for Hard Sphere- A verification of Analytical Results by Computer Simulations", *Acta Physica Polonica*, Vol. A74, No. 6, 1988, pp. 811-819.
- ²⁰ Bird, G.A., "General Programs for Numerical Simulation of Rarefied Gas Flows", G.A.B. Consulting Pty. Ltd., Killara, Australia, 1988.
- ²¹ Park, C., "Assessment of a Two Temperature Kinetic Model for Dissociating and Weakly Ionizing Nitrogen", *Journal of Thermophysics and Heat Transfer*, Vol. 2, No. 1, 1988, pp. 8-16.
- ²² Candler, G., "On the Computation of Shock Shapes in Nonequilibrium Hypersonic Flows", AIAA Paper 89-0312, January 1989.

Table 1. Freestream conditions.

| Altitude (km) | U_∞ (km/s) | Density (kg/m ³) | T_∞ (K) | X_{O_2} | X_{N_2} |
|---------------|-------------------|------------------------------|----------------|-----------|-----------|
| 90 | 7.5 | 3.418×10^{-6} | 188.0 | 0.23 | 0.77 |

Table 2. Parameters for Rotational Energy Exchange.

| Species | $(Z_R)_\infty$ | T^* (K) | Z_t |
|----------------|----------------|-----------|-------|
| N ₂ | 23.3 | 91.5 | 1.5 |
| O ₂ | 16.5 | 113.5 | 1.5 |
| NO | 19.5 | 100.0 | 1.5 |

Table 3. Parameters for Vibrational Energy Exchange.

| Species | Z_o | g^* (m/s) | σ_v (m ²) |
|----------------|-----------------------|-------------|------------------------------|
| N ₂ | 8.30×10^{10} | 43300 | 10^{-20} |
| O ₂ | 1.50×10^{11} | 18200 | 10^{-20} |
| NO | 1.51×10^{11} | 6400 | 10^{-20} |

Table 4. Results For Restricted Rotational Contributions To Chemical Reactions.

| ϕ_R | ϕ_v | Shock Standoff (m) | C_H | Surface Mass Fraction of N ₂ |
|----------|----------|--------------------|-------|---|
| 0.2 | 0.02 | 0.110 | 0.177 | 0.561 |
| Eq.(2) | 0.02 | 0.113 | 0.178 | 0.547 |
| Eq.(2) | Eq.(8) | 0.115 | 0.180 | 0.540 |

Table 5. Results For Different Rotational Contributions To Chemical Reactions.

| Rotational Contribution | ϕ_R | ϕ_v | Shock Standoff (m) | C_H | Surface Mass Fraction of N ₂ |
|-------------------------|----------|----------|--------------------|-------|---|
| Restricted | 0.2 | 0.02 | 0.110 | 0.177 | 0.561 |
| Full | 0.2 | 0.02 | 0.110 | 0.177 | 0.552 |
| Full | Eq.(2) | 0.02 | 0.116 | 0.182 | 0.530 |
| Full | Eq.(2) | Eq.(8) | 0.118 | 0.188 | 0.506 |

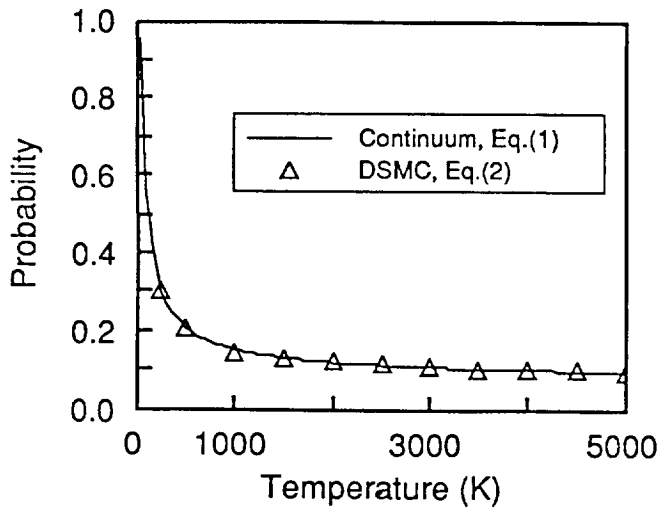


Fig. 1. Rotational energy exchange probability as a function of temperature.

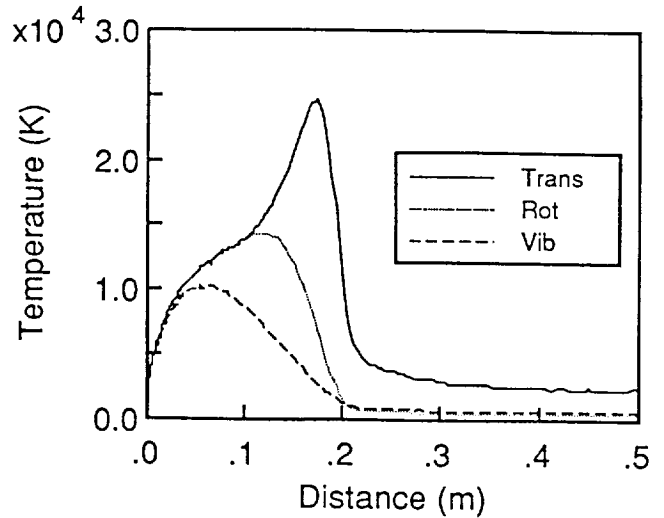


Fig. 4a. Thermal nonequilibrium along stagnation streamline for constant exchange probabilities.

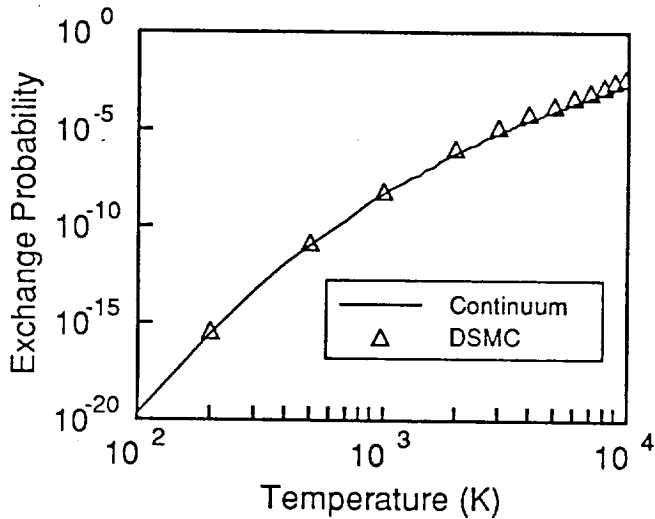


Fig. 2. Vibrational energy exchange probability as a function of temperature.

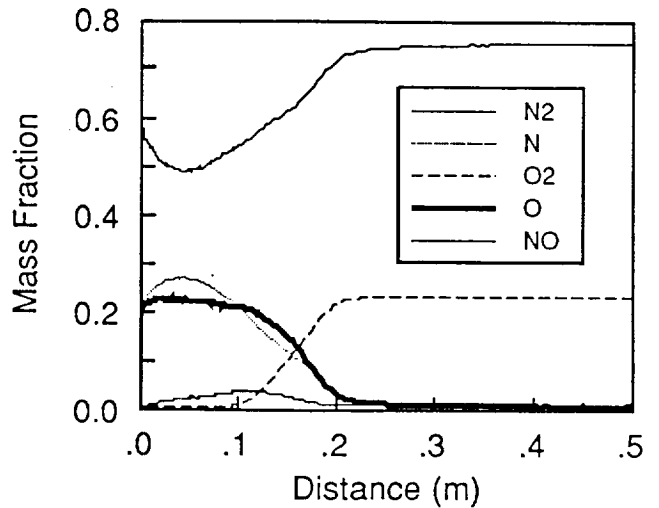


Fig. 4b. Species mass fractions along stagnation streamline for constant exchange probabilities.

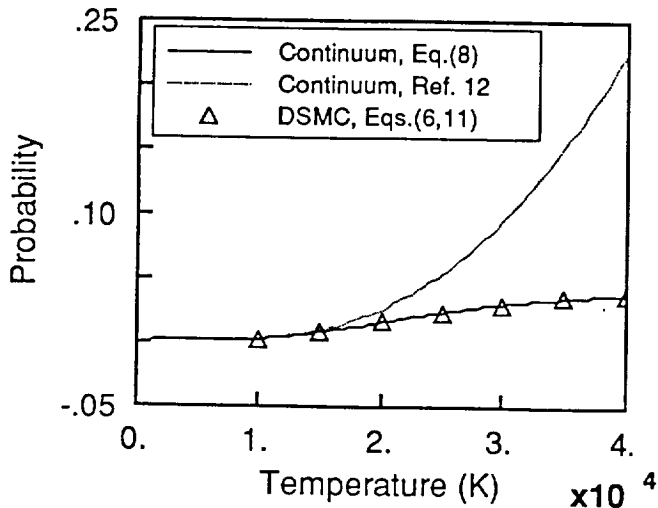


Fig. 3. Vibrational energy exchange probability with Parks empirical correction.

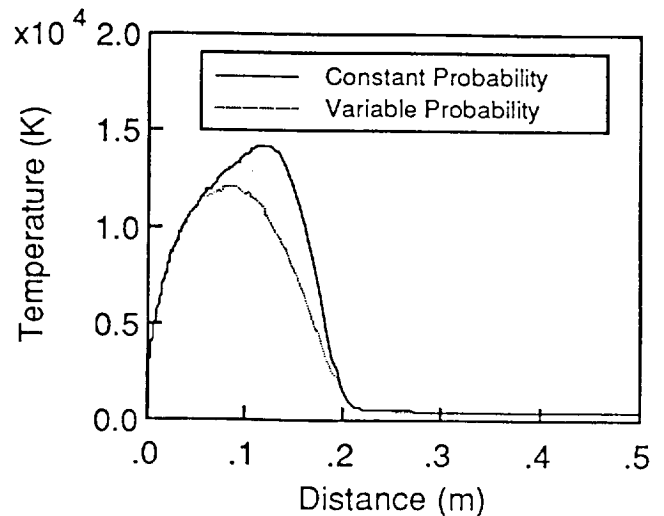


Fig. 5. Comparison of rotational temperature profiles for different rotational energy exchange models.

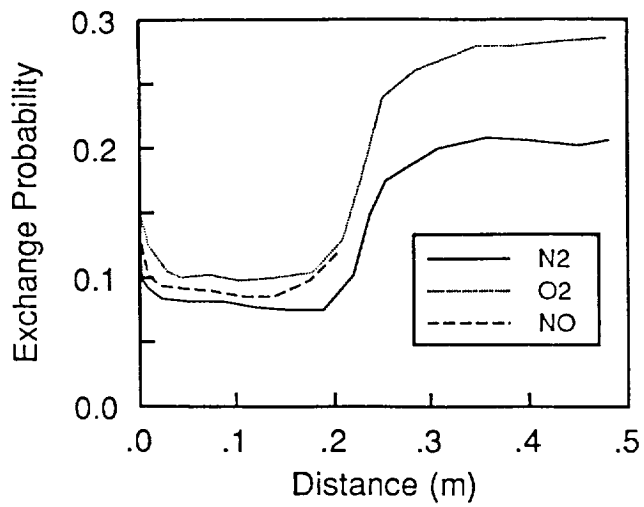


Fig. 6. Variation of rotational energy exchange probabilities.

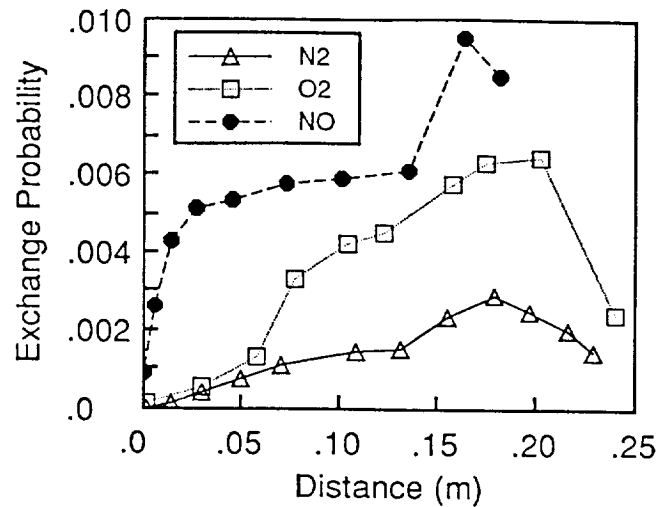


Fig. 9. Variation of vibrational energy exchange probabilities.

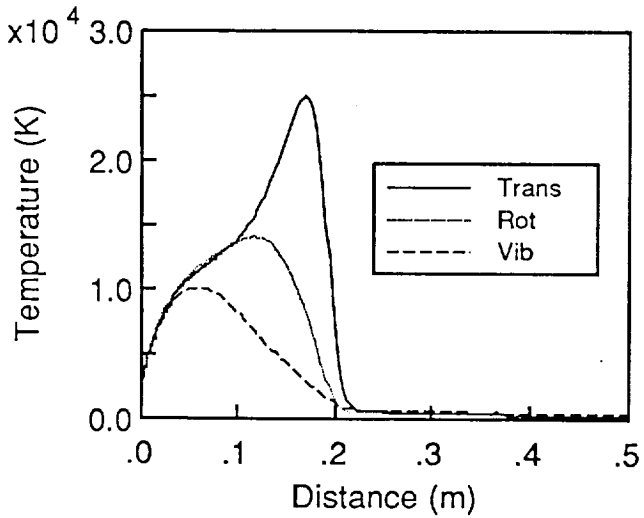


Fig. 7. Thermal nonequilibrium of molecular nitrogen.

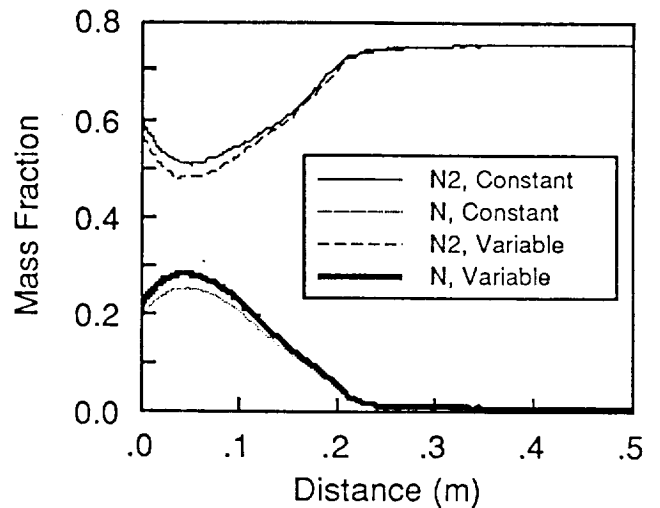


Fig. 10. Comparison of mass fractions of molecular and atomic nitrogen for different energy exchange models.

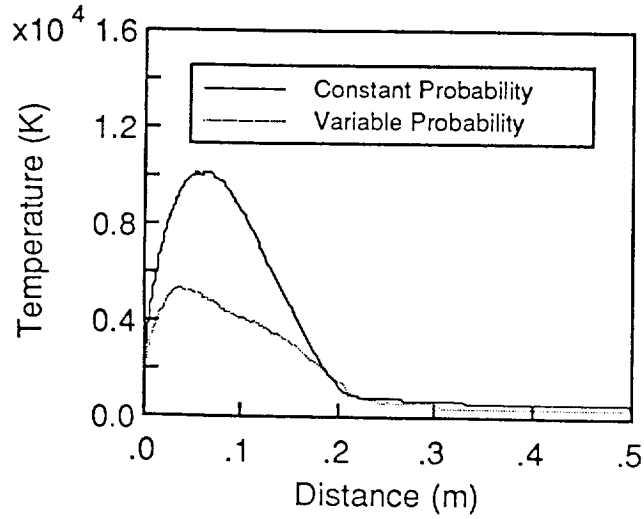


Fig. 8. Comparison of vibrational temperature profiles for different vibrational energy exchange models.

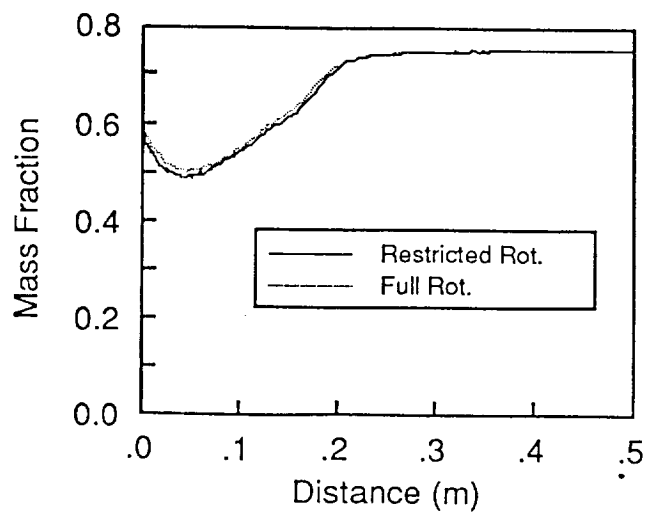


Fig. 11. Comparison of mass fraction of molecular nitrogen for different steric factors.

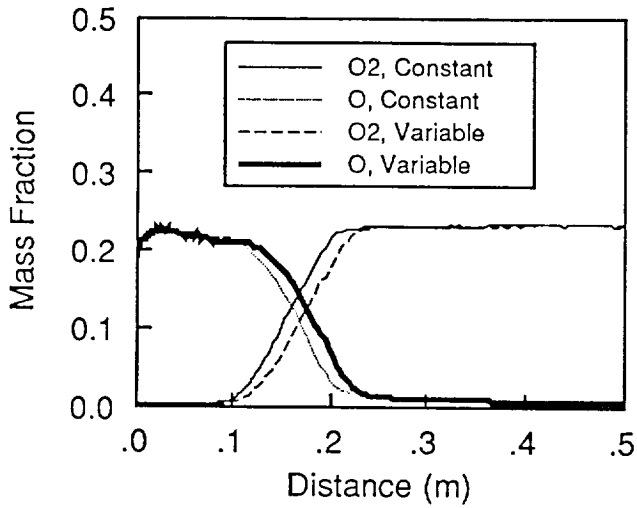


Fig. 12. Comparison of mass fractions of molecular and atomic oxygen for different energy exchange models with full rotational contribution to the steric factor.

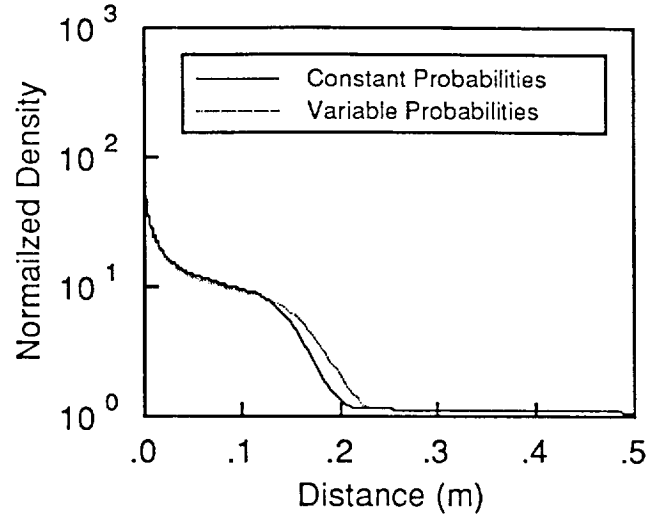


Fig. 14. Comparison of density for different energy exchange models with full rotational contribution to the steric factor.

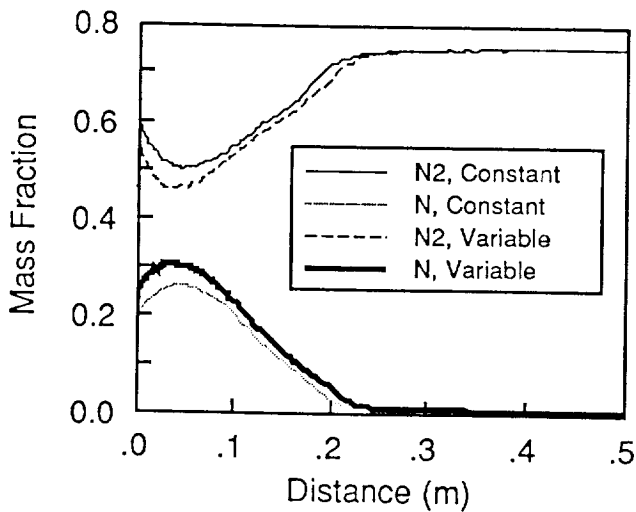


Fig. 13. Comparison of mass fractions of molecular and atomic nitrogen for different energy exchange models with full rotational contribution to the steric factor.

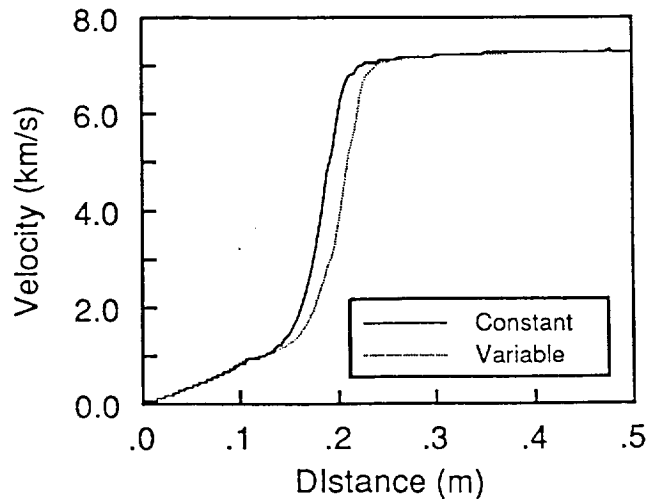


Fig. 15. Comparison of velocity for different energy exchange models with full rotational contribution to the steric factor.